

AdaNN: Adaptive Neural Network-based Equalizer via Online Semi-supervised Learning for High-speed Optical Fiber Communication

Qingyi Zhou, and Chuanchuan Yang, *Senior Member, IEEE*

Abstract—The demand for high speed data transmission has increased rapidly over the past few years, leading to the development of advanced optical communication techniques. At this point, nonlinear effects caused by optical fiber characteristics and non-ideal devices are becoming significant, limiting the achievable transmission distance and channel capacity of high speed optical communication systems. Such effects cannot be equalized efficiently using conventional equalizers. In the past few years, multiple equalizers based on neural network (NN) have been proposed to recover signal from nonlinear distortions. However, previous experiments mainly focused on achieving low bit error rate (BER) on certain dataset with an offline-trained NN, neglecting the generalization ability of NN-based equalizer when the properties of optical link change. Few people are committed to developing efficient online training scheme, which hinders the application of NN-based equalizers. In this paper, we've proposed an adaptive online training scheme, which can be used to fine-tune parameters of NN-based equalizer without the help of training sequence. The online training scheme originates from decision-directed adaptive equalization. By combining it with data augmentation and virtual adversarial training, we've successfully increased the convergence speed by 4.5 times. The proposed adaptive NN-based equalizer is called "AdaNN". Its BER has been evaluated over a 56 Gb/s PAM4-modulated VCSEL-MMF optical link, showing performance improvement compared with non-adaptive NN-based equalizer and conventional MLSE.

Index Terms—Optical fiber communication, Adaptive nonlinear equalizer, Neural network, Semi-supervised learning.

I. INTRODUCTION

WITH the continuous development of the Internet, higher bandwidth data transmission is required. Advanced modulation techniques together with novel algorithms have emerged to fulfill the requirements. Digital signal processing (DSP) is quite essential for improving the bit-error-rate (BER) performance and raising the optical links transmission rate. Real-time DSP has been considered a viable solution for expanding available bandwidth and capacity in next generation networks.

In order to achieve large transmission capacity in short-range optical interconnects, researchers have tried out a variety of conventional DSP techniques. With feed forward

equalization (FFE), the data rate of non-return-to-zero (NRZ) have reached 71 Gb/s [1]. Other conventional equalization techniques, such as decision feedback equalizer (DFE) and maximum likelihood sequence estimator (MLSE), have also been utilized [2]-[5]. By utilizing both the pre-emphasis at transmitter and equalization at receiver, 94 Gb/s and 107 Gb/s PAM-4 transmission have been demonstrated by K. Szczerba et al. [6] and J. Lavrencik et al. [7] respectively.

Researchers have also been trying to exploit the potential of DSP algorithms for long-reach optical fiber communication systems. Volterra nonlinear equalizer (VNLE) has been utilized long ago to mitigate nonlinear channel distortions [8]. A few works have been done in order to lower the high complexity of VNLE [9], [10]. Several other nonlinearity compensation technologies have also been investigated, such as digital back-propagation (DBP) [11], perturbation-based compensation [12], and nonlinear Kalman filter [13].

All the above-mentioned DSP algorithms are designed on rich expert knowledge, and some can be proved optimal for tractable mathematical models. However, many nonlinearities (modulation nonlinearity together with square law detection) that exist in practical systems can only be approximately captured and are difficult to compensate with conventional DSP techniques [14]. In order to solve this problem, many DSP algorithms based on neural network have been proposed recently, including artificial neural network (ANN) based equalizer [15], [16], convolutional neural network (CNN) based equalizer [17] and recurrent neural network (RNN) based equalizer [18], [19]. In [19] we also proposed a variant named "Half-RNN", whose computational complexity is 40% lower than normal RNN while maintaining very similar BER performance. Implemented in different optical communication systems, these NN-based equalizers have not only reached better BER performance, but also shown excellent capability of mitigating system nonlinearity.

Although various researchers report to have achieved better BER performance using NN-based equalizers, whether NN-based equalizer can replace conventional equalizer under certain conditions still remains a question. One important problem is that it's very difficult for NN-based equalizers to generalize over varied channel condition. In an actual communication system, the external environment and channel parameters change slowly, and the probability distribution of received data can differ from the distribution of training dataset utilized at the offline training stage. Therefore, while an NN-based equalizer trained offline can perform better on training set/test

Manuscript received xx xx, xxxx; revised xx xx, xxxx (*Corresponding author: Chuanchuan Yang*).

The authors are with the State Key Laboratory of Advanced Optical Communication Systems and Networks, Department of Electronics, Peking University, Beijing 100871, China (e-mail: zhouqingyi@pku.edu.cn, yangchuanchuan@pku.edu.cn). This work is funded by National Key R&D Program of China under Grant 2018YFB180066-02 and Joint Fund of the Ministry of Education under Grant 6141A02033347.

set, which is obtained under specific condition, it suffers from severe performance degradation when the distribution of received data “drifts away” from the original one [20]. On the other hand, it is far too costly to train different networks for different communication systems. However, to the best of our knowledge, existing work on NN-based equalizers still require offline training with pre-collected large dataset. Due to the lack of the ability to adjust model parameters adaptively, these equalizers are not practical.

In order to maintain good BER performance of NN under a more realistic scenario, it’s important to develop an adaptive NN-based equalizer. We expect that a new training scheme, which does not rely on massive amount of collected labeled data and can perform well in an online manner, can be utilized. For conventional equalizers (FFE, DFE, MLSE, Volterra, etc.) it appears quite normal to estimate the channel response adaptively with the help of short training sequence. Unfortunately, we’ve found that, when the short training sequence is provided to an NN-based equalizer, the equalizer still suffers from degraded BER performance. The main reason is that an NN with hundreds of parameters requires large amount of training data, and is very likely to overfit when trained on the short, pseudo-random training sequence [21].

In this paper, we propose an adaptive online training scheme, which can be used to fine-tune NN-based equalizer *without* the help of training sequence. During the online stage, our NN is similar to a decision-directed adaptive equalizer. Although our NN still needs to be trained with labeled training set at the offline training stage, at the online stage no labeled data needs to be provided. Rather, we collect recently received data using a sliding-window, then fine-tune all the parameters in our neural network with the help of the unlabeled data collected from the window. The whole process can actually be viewed as semi-supervised learning. By combining virtual adversarial training (VAT) with data augmentation, a loss function named “Aug-VAT” is proposed which outperforms other types of loss functions in this task and leads to a 4.5 times speedup [22]–[25]. Different optimization algorithms are also compared, revealing the importance of choosing appropriate optimizer. The proposed adaptive NN-based equalizer is called “AdaNN” for short, and the performance is evaluated in a 56 Gb/s PAM4-modulated VCSEL optical link. Our experimental results indicate that by introducing AdaNN, the BER performance can be improved compared with both non-adaptive NN-based equalizers (ANN, RNN) and conventional MLSE. We also give detailed complexity analysis. Conclusions can be reached that without the help of training sequence, it is possible to construct adaptive NN-based equalizer with acceptable computational cost, justifying the significance of our work.

The rest of this paper can be organized as follows. Section II provides a detailed introduction of our proposed online semi-supervised training scheme. In Section III, sliding-window is proposed to collect recently received data. The influence of the sliding-window’s step size is researched. In Section IV, the computational complexity of AdaNN’s online training process is analyzed. In section V, the BER performance of AdaNN, MLSE, and other non-adaptive NN-based equalizers, are tested

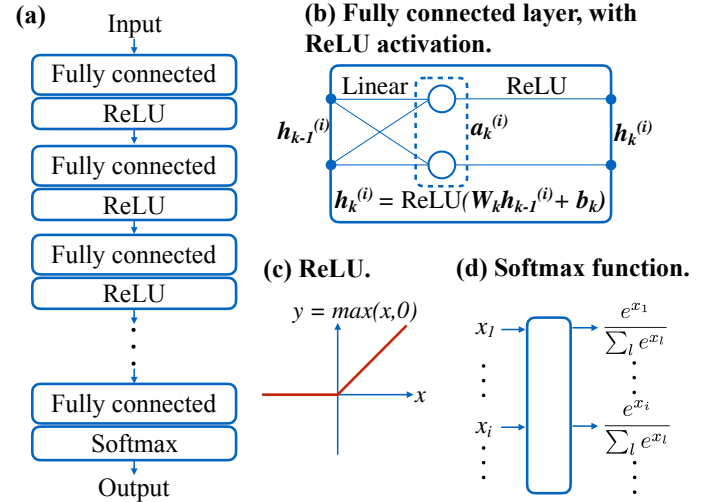


Fig. 1: (a) The structure of NN-based equalizer evaluated in this paper, including input layer, hidden layers and output layer. (b) Fully-connected layer, with ReLU activation. Note that only a few neurons are explicitly drawn. (c) The ReLU activation function. (d) The definition of softmax function.

and compared. Section VI concludes the paper.

II. ADANN: ONLINE TRAINING BASED ON SEMI-SUPERVISED LEARNING

A. Nonlinear equalizer based on NN

Without loss of generality, the NN we use contains an input layer, an output layer, and several hidden layers (each hidden layer contains R neurons), as shown in Fig. 1(a)(b). The total number of layers contained in this NN is denoted as l_{NN} . For the i -th symbol, the relationship between adjacent fully-connected layers (denoted as layer k and $k - 1$, where $k \in \{1, \dots, l_{NN} - 1\}$) follows

$$a_k^{(i)} = W_k h_{k-1}^{(i)} + b_k, \quad (1)$$

$$h_k^{(i)} = \sigma(a_k^{(i)}), \quad (2)$$

where W_k is fully-connected weight matrix whose size is $R \times R$, and b_k is bias vector for layer k . Function $\sigma(\cdot)$ stands for activation function, with softmax chosen for the output layer and ReLU for all the hidden layers. The definition of different activation functions are given in Fig. 1(c)(d).

1) *Offline Training Stage:* At the offline training stage, we need to find appropriate weights and biases by minimizing the loss function. The loss function has the form of cross-entropy, which is widely used in machine learning when dealing with multi-class classification [26]. Denote the total number of symbols contained in the sequence as N_{seq} . The training process can be formulated as

$$\min_{\{W_k, b_k\}} L_{loss} = \min_{\{W_k, b_k\}} \left(-\frac{1}{N_{seq}} \sum_{i=1}^{N_{seq}} \sum_{j=1}^M y_j^{(i)} \ln(o_j^{(i)}) \right), \quad (3)$$

where M means for PAM- M , a symbol only belongs to one of M classes. The loss function L_{loss} measures the difference between predicted probability $o^{(i)}$ and ground truth $y^{(i)}$. The whole training dataset is divided into small batches, each

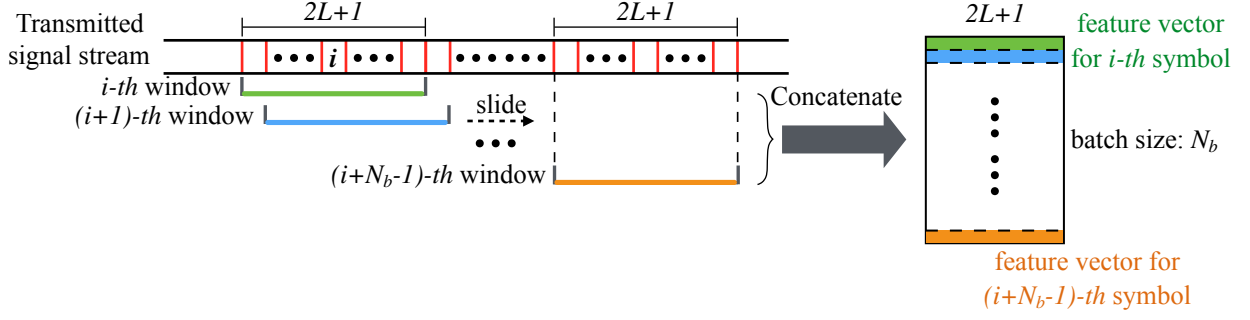


Fig. 2: A schematic illustration of the sliding window. The sliding window is used to collect mini-batches. The model parameters can be updated only if a batch containing N_b samples has been collected.

containing a small portion of all N_{seq} training samples. The network parameters are updated iteratively using Stochastic Gradient Descent (SGD) optimizer with momentum, which is much faster compared with vanilla SGD [26]. At step t , its parameter update rule is given by

$$\begin{cases} \mathbf{V}_{t+1} = \beta \mathbf{V}_t - \alpha \frac{\partial L_t}{\partial \boldsymbol{\theta}_t}, \\ \boldsymbol{\theta}_{t+1} = \boldsymbol{\theta}_t + \mathbf{V}_{t+1}, \end{cases} \quad (4)$$

where $\boldsymbol{\theta}_t$ includes all trainable parameters (weights and biases), L_t denotes the loss function L_{loss} on a single batch B_t , \mathbf{V}_t denotes the accumulation of historical gradient, α denotes the learning rate, and $\beta \in (0, 1)$ is the rate of moving average decay.

2) *Equalizing Process:* During equalization, we denote the received signal sequence after interpolation and zero-mean normalization as $\hat{\mathbf{r}} = [\hat{\mathbf{r}}_1, \hat{\mathbf{r}}_2, \dots, \hat{\mathbf{r}}_{N_{seq}}]$, where vectors $\hat{\mathbf{r}}_1, \dots, \hat{\mathbf{r}}_{N_{seq}}$ correspond to N_{seq} received symbols (following chronological order). The feature vector $\mathbf{v}^{(i)}$ for the i -th symbol is constructed as

$$\mathbf{v}^{(i)} = [\hat{\mathbf{r}}_{i-L}, \dots, \hat{\mathbf{r}}_i, \dots, \hat{\mathbf{r}}_{i+L}]. \quad (5)$$

If we denote the interpolation multiple as Γ , then the dimension of input feature vector $\mathbf{v}^{(i)}$ is $\Gamma(2L + 1)$. The input-output relationship is the same as Eq. (1)(2). Since normal NN works non-adaptively, all the weights and biases in the network remain unchanged during equalization, which is not the case for AdaNN.

B. Proposed AdaNN training scheme

Our goal is to classify PAM- M signals into M classes correctly. For such a multi-class classification problem, data can be either “labeled” or “unlabeled”. The term “labeled” means that for an input vector $\mathbf{x}^{(i)}$, the true label $\mathbf{y}^{(i)}$ (which is an one-hot vector) is provided. “Unlabeled” on the other hand, means that no true label is provided and the network does not know the exact classification result.

In practice, the properties of optical link are changing slowly, and the distribution of received data can “drift away” over time, causing performance degradation for NN-based equalizer. A proper online training scheme is urgently needed in order to solve these problems. During online training stage, it is impossible to gather large amount of labeled data. In practice it is only possible that the transmitter provide

short training sequences for channel estimation/parameter fine-tuning. Unfortunately, short training sequences are not enough for training a neural network, since the complicated network is likely to over-fit the small training set (using pseudo-randomly generated training sequence may also cause serious over-fitting [21]).

A possible solution is that, although we do not know the exact labels at the receiver, we can make use of the distribution of received signals to monitor the “drift away” process and use such information to fine-tune our equalizer. Here the concept of semi-supervised learning naturally arises. Semi-supervised learning is a class of machine learning tasks that make use of unlabeled data for training (typically a small amount of labeled data with a large amount of unlabeled data). Semi-supervised learning falls between unsupervised learning (without any labeled training data) and supervised learning (with all training data properly labeled). Unlabeled data helps us by providing information about the probability density distribution of input vectors, denoted as $p(\mathbf{x})$ [22].

Based on the idea of semi-supervised learning, we now explain the process of proposed AdaNN. The offline training is described by Eq. (3)(4), so we focus on the online training stage in this part. First of all, during online training stage, a sliding window is utilized to collect data, which is illustrated in Fig. 2. The window, containing $2L + 1$ symbols and denoted as bold line, slides on the received signal sequence at the step of N_b . Therefore at each step t , N_b input feature vectors $\mathbf{v}^{(1)}, \mathbf{v}^{(2)}, \dots, \mathbf{v}^{(N_b)}$ are collected and forms a mini-batch. The total number of batches is denoted as N_{batch} . A gradient \mathbf{g}_t should be calculated based on the loss function of this mini-batch, and the parameters should then be updated.

In order to decide the form of the loss function, we observe that:

- (1) When no labels are provided, the NN can work adaptively under decision-directed mode, but the convergence speed is very slow.
- (2) By adding Gaussian noise on the input feature vector, the training can be accelerated.
- (3) Using VAT will also speed up the convergence of online training process.

Therefore, in our proposed training scheme for AdaNN, Π -model [24] and VAT [25] are combined directly. This final form of loss function is named as “Augmented Virtual Adversarial Training”, or “Aug-VAT” for short. Fig. 3 shows

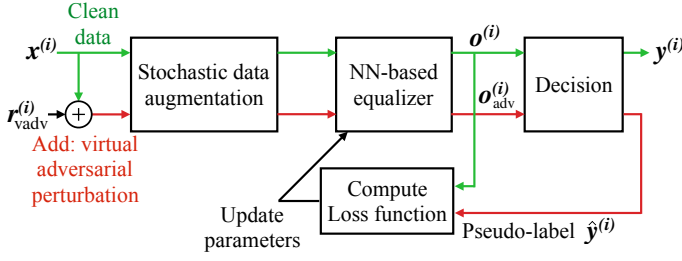


Fig. 3: The general structure of AdaNN, with Aug-VAT serves as loss function. When true labels are not provided, the parameters in the NN-based equalizer can be updated with the help of pseudo-label $\hat{y}^{(i)}$.

the general structure of AdaNN with Aug-VAT. The detailed algorithm will also be given in this part.

II model encourages consistent network output between two realizations of the same input vector, under two different data augmentation conditions. Denote $g_\sigma(\mathbf{v})$ as the input augmentation function. The augmentation is done by generating a random vector $\boldsymbol{\eta}$ using i.i.d Gaussian distribution and add it on \mathbf{v} :

$$g_\sigma(\mathbf{v}) = \mathbf{v} + \boldsymbol{\eta}, \quad (6)$$

where all $\boldsymbol{\eta}$'s components $\eta_k \in \mathcal{N}(0, \sigma)$, and index $k \in \{1, \dots, \Gamma(2L+1)\}$. Note that the standard deviation of elements in \mathbf{v} should be close to 1 after normalization, which helps us choose hyper-parameter σ .

When using Aug-VAT as loss function in AdaNN, every single input feature vector \mathbf{v} should first be replaced using $g_\sigma(\mathbf{v})$, then serve as the input feature vector in VAT. VAT is closely related to adversarial training [27]. The adversarial perturbation for the i -th input vector can be defined as

$$\mathbf{r}_{\text{adv}}^{(i)} = \arg \max_{\mathbf{r}; \|\mathbf{r}\| \leq \epsilon} \left\{ - \sum_{j=1}^M y_j^{(i)} \ln[(\text{NN}_{\theta}(g_\sigma(\mathbf{v}^{(i)} + \mathbf{r})))_j] \right\}. \quad (7)$$

This equation implies that by adding a small perturbation $\mathbf{r}_{\text{adv}}^{(i)}$ (satisfying $\|\mathbf{r}_{\text{adv}}^{(i)}\| \leq \epsilon$) on $\mathbf{v}^{(i)}$, the loss function calculated using the perturbed input tend to increase. ‘‘Adversarial training’’ means that for each input vector, the adversarial perturbation is calculated and added onto the ‘‘clean’’ input vector, and during training the loss function is always calculated based on the perturbed input vectors rather than the clean ones, so that NN’s robustness can be improved. However, when full label information $\mathbf{y}^{(i)}$ is not available, \mathbf{r}_{adv} can only be approximated by computing \mathbf{r}_{vadv} , which is derived efficiently by using one-time power iteration method (see Algorithm 1).

By combining data augmentation with VAT, the final pseudocode of our proposed AdaNN online training scheme (with Aug-VAT as loss function) is given in Algorithm 2. We’ve also drawn the flow chart of AdaNN algorithm in Fig. 4, for the sake of clarity. At step t , the gradient \mathbf{g}_t is accumulated before all the data in batch B_t have been utilized. After that, parameters $\boldsymbol{\theta}_t$ should be updated using gradient-based optimizer. Here, all gradient-based optimization algorithms can be written in the following general form [28]:

$$\boldsymbol{\theta}_{t+1} = \boldsymbol{\theta}_t - \frac{\alpha_t}{\psi(\mathbf{g}_1, \dots, \mathbf{g}_t)} \phi(\mathbf{g}_1, \dots, \mathbf{g}_t), \quad (8)$$

Algorithm 1 Virtual adversarial perturbation

Require: $\mathbf{v}^{(i)}$ = the input vectors collected by sliding window ($i = 1, 2, \dots, N_b \cdot N_{\text{batch}}$)
Require: $\boldsymbol{\theta}$ = parameters of the offline-trained network
Require: ξ = step size of gradient estimation
Require: ϵ = length of adversarial perturbation

- 1: Generate random vector $\mathbf{d}^{(i)}$ using i.i.d standard Gaussian distribution.
- 2: $\mathbf{r} \leftarrow \xi \mathbf{d}^{(i)}$
- 3: $\mathbf{o}^{(i)} \leftarrow \text{NN}_{\boldsymbol{\theta}}(g_\sigma(\mathbf{v}^{(i)}))$
- 4: $\mathbf{o}'^{(i)} \leftarrow \text{NN}_{\boldsymbol{\theta}}(g_\sigma(\mathbf{v}^{(i)} + \mathbf{r}))$
- 5: Compute $L_{\text{loss}} = D_{KL}(\mathbf{o}^{(i)} \parallel \mathbf{o}'^{(i)}) \triangleright$ the difference between two output vectors can be quantified using Kullback-Leibler divergence
- 6: $\mathbf{g}^{(i)} \leftarrow \nabla_{\mathbf{r}} L_{\text{loss}}$
- 7: $\mathbf{r}_{\text{vadv}}^{(i)} \leftarrow \mathbf{g}^{(i)} / \|\mathbf{g}^{(i)}\|_2$
- 8: $\mathbf{r}_{\text{vadv}}^{(i)} \leftarrow \epsilon \cdot \mathbf{r}_{\text{vadv}}^{(i)}$

Algorithm 2 AdaNN

Require: $\mathbf{v}^{(i)}$ = the input vectors collected by sliding window ($i = 1, 2, \dots, N_b \cdot N_{\text{batch}}$)
Require: $\boldsymbol{\theta}_1$ = parameters of the offline-trained network
Require: $g_\sigma(\cdot)$ = add Gaussian noise with deviation σ

- 1: **for** t in $[1, N_{\text{batch}}]$ **do**
- 2: **for** i in $[1, N_b]$ **do**
- 3: $\mathbf{o}^{(i)} \leftarrow \text{NN}_{\boldsymbol{\theta}_t}(g_\sigma(\mathbf{v}^{(i)}))$
- 4: $l \leftarrow \arg \max_k o_k^{(i)} \triangleright$ predicted label
- 5: compute $\mathbf{r}_{\text{vadv}}^{(i)}$ using Algorithm 1
- 6: $\mathbf{o}_{\text{adv}}^{(i)} \leftarrow \text{NN}_{\boldsymbol{\theta}_t}(g_\sigma(\mathbf{v}^{(i)} + \mathbf{r}_{\text{vadv}}^{(i)}))$
- 7: $l_{\text{adv}} \leftarrow \arg \max_k o_{\text{adv},k}^{(i)} \triangleright$ perturbed label
- 8: $\hat{y}_{l_{\text{adv}}}^{(i)} = 1 \triangleright$ one-hot perturbed label vector
- 9: $L_{\text{loss}} \leftarrow L_{\text{loss}} - \frac{1}{N_b} \sum_{j=1}^M \hat{y}_j^{(i)} \ln(o_j^{(i)}) \triangleright$ update loss function
- 10: **end for**
- 11: $\mathbf{g}_t \leftarrow \frac{\partial L_{\text{loss}}}{\partial \boldsymbol{\theta}_t} \triangleright$ compute gradient on batch
- 12: update $\boldsymbol{\theta}_t$ using gradient-based optimizer (e.g., Adam)
- 13: **end for**

where \mathbf{g}_t represents the gradient obtained at the t -th time step, $\alpha_t / \psi(\mathbf{g}_1, \dots, \mathbf{g}_t)$ denotes the adaptive learning rate, and $\phi(\mathbf{g}_1, \dots, \mathbf{g}_t)$ is the gradient estimation. For example, choosing $\alpha_t = \alpha$, $\psi(\mathbf{g}_1, \dots, \mathbf{g}_t) = 1$ and $\phi(\mathbf{g}_1, \dots, \mathbf{g}_t) = \mathbf{g}_t$ simply leads to the vanilla SGD.

C. Other choices for loss function

When labels are not provided, $y_j^{(i)}$ in Eq. (3) should be replaced with pseudo-label $\hat{y}_j^{(i)}$. The loss function of a single batch still has the cross-entropy form

$$L_{\text{loss}} = -\frac{1}{N_b} \sum_{i=1}^{N_b} \sum_{j=1}^M \hat{y}_j^{(i)} \ln(o_j^{(i)}). \quad (9)$$

Pseudo-label $\hat{y}_j^{(i)}$ can be obtained in different ways, corresponding to different loss functions. In the last subsection,

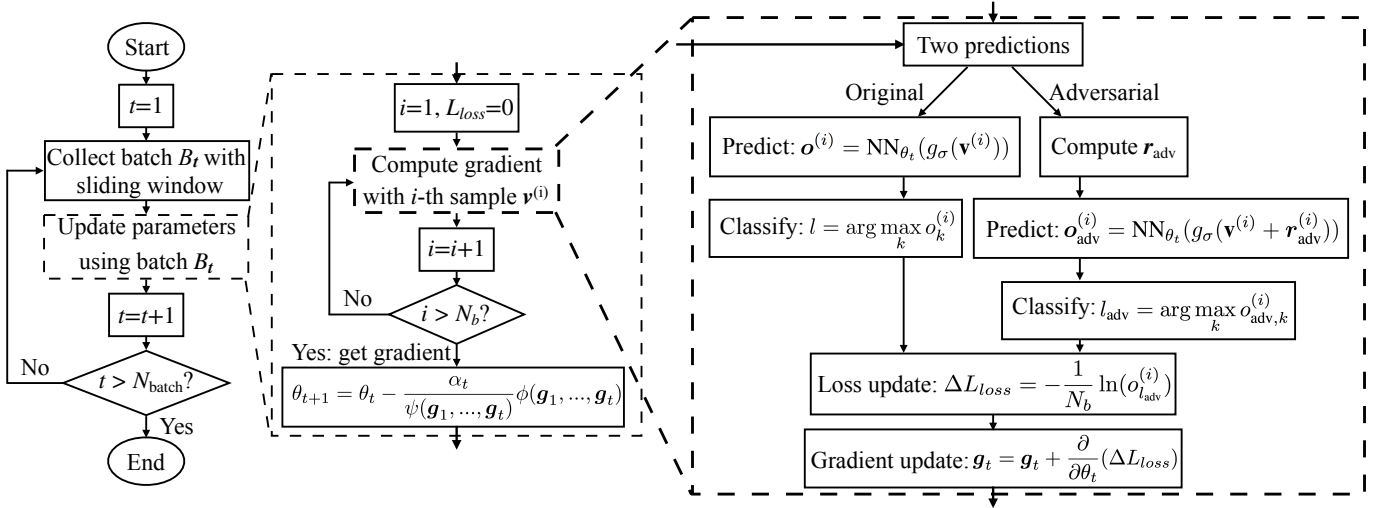


Fig. 4: The complete flow chart of the AdaNN process. The box with thinner dashed lines represents the processing of a single batch. The box with thicker dashed lines, on the other hand, represents the processing of the i -th sample in the batch.

we've already proposed Aug-VAT loss function, which combines Π -model with VAT. In fact, vanilla self-training, Π -model and VAT can be used alone. Therefore, in this part the BER performance of these three loss functions are compared with that of Aug-VAT.

1) *Self-training*: For the i -th input feature vector $\mathbf{v}^{(i)}$, the output probability vector $\mathbf{o}^{(i)} = \text{NN}_{\theta}(\mathbf{v}^{(i)})$. The pseudo-label $\hat{\mathbf{y}}^{(i)}$ can be derived by

$$\hat{y}_j^{(i)} = \begin{cases} 1, & \text{if } j = \arg \max_k (o_k^{(i)}), \\ 0, & \text{otherwise.} \end{cases} \quad (10)$$

This training scheme is similar to the decision-directed mode of conventional adaptive equalizers, and therefore serves as a baseline.

2) *Π -model only*: The main difference between Π -model and self-training lies in data augmentation. The output probability vector $\mathbf{o}^{(i)} = \text{NN}_{\theta}(g_{\sigma}(\mathbf{v}^{(i)}))$, where $g_{\sigma}(\cdot)$ follows Eq. (6). The derivation of $\hat{\mathbf{y}}^{(i)}$ is the same as Eq. (10).

3) *Virtual adversarial training only*: When using vanilla VAT, the output probability vector $\mathbf{o}_{\text{adv}}^{(i)} = \text{NN}_{\theta}(\mathbf{v}^{(i)} + \mathbf{r}_{\text{adv}}^{(i)})$, where $\mathbf{r}_{\text{adv}}^{(i)}$ is the virtual adversarial perturbation vector calculated from Algorithm 1. The derivation of $\hat{\mathbf{y}}^{(i)}$ is the same as Eq. (10).

In order to compare all these different loss functions, we've conducted experiments with the help of a 56 Gb/s PAM4-modulated VCSEL optical link. The BER curves are given in this part. The VCSEL based optical interconnect system is depicted in Fig. 5. The system mainly consists of a directly modulated 850-nm VCSEL, 100-m OM4 MMF, and a photodiode (PD). The modulated optical signal is detected by the PD, then transformed into baseband electrical signals. The baseband signal is then sampled using a high-speed real-time digital signal oscilloscope (DSO) with sampling rate of 160 GSa/s. We first 4x resample the received signal as stated in [29]. The signal is then processed using zero-mean normalization, which yields $\hat{\mathbf{s}} = [\hat{s}_1, \dots, \hat{s}_{N_{\text{seq}}}]$. To construct

the input feature vector $\mathbf{x}^{(i)}$ for the i -th symbol, we wrap $\hat{\mathbf{s}}_i$ with its $2L$ adjacent vectors together as

$$\mathbf{x}^{(i)} = [\hat{\mathbf{s}}_{i-L}, \dots, \hat{\mathbf{s}}_i, \dots, \hat{\mathbf{s}}_{i+L}]. \quad (11)$$

In our experiments, the 850 nm VCSEL is New Focus[®] 1784 [30], while PD is New Focus[®] 1484-A-50 [31]. The -3 dB bandwidth of VCSEL and PD are 18 GHz and 22 GHz respectively. The OM4 MMF is chosen as YOFC[®] MaxBand[®] OM4 bend insensitive multimode fiber, with an over filled launch (OFL) bandwidth of 4394 MHz \times km. At receiver side, the DSO is Agilent DSAX96204Q, with sampling rate of 160 GSa/s.

We have generated two sets of PAM-4 symbols with Bit-pattern Generator (BPG) of SHF 12104A, using random pattern (56 Gb/s). Each of the two datasets (denoted as set1 and set2) contains 2^{20} PAM-4 symbols. Set2 was collected 56 hours after we collected set1. During the time interval, the VCSEL was turned off and on, so that the two datasets are heterogeneous. Our NN-based equalizer with 4 hidden layers ($l_{\text{NN}} = 6$) is first trained offline using 25% data in set1. The tap number of NN is fixed as $L = 5$. For the offline training stage, the batch size is fixed as 16384. We choose to use Momentum SGD during offline training. The moving average decay β takes the default value $\beta = 0.9$ implemented in Keras [32]. The initial value of learning rate α is chosen to be 0.004. The model is trained for 200 epochs, ensuring good convergence and a BER lower than 10^{-3} .

During online stage, a sliding window is utilized to collect data, as Fig. 2 shows. Set1 and set2 are concatenated, and the equalizer processes set1 and set2 sequentially. The batch size for online training is fixed to be $N_b = 16384$ ($N_{\text{batch}} = 256$). The optimizer is Momentum SGD, with $\beta = 0.9$ and initial learning rate $\alpha = 0.01$. When processing set1 and set2 sequentially, the BER for set1 will remain relatively low, while for set2 the BER will increase abruptly. By utilizing an online training scheme, hopefully the BER will then decrease to a low level. Here we present the adaptive training results for all the 4 different loss functions. We mainly focus on two quantities:

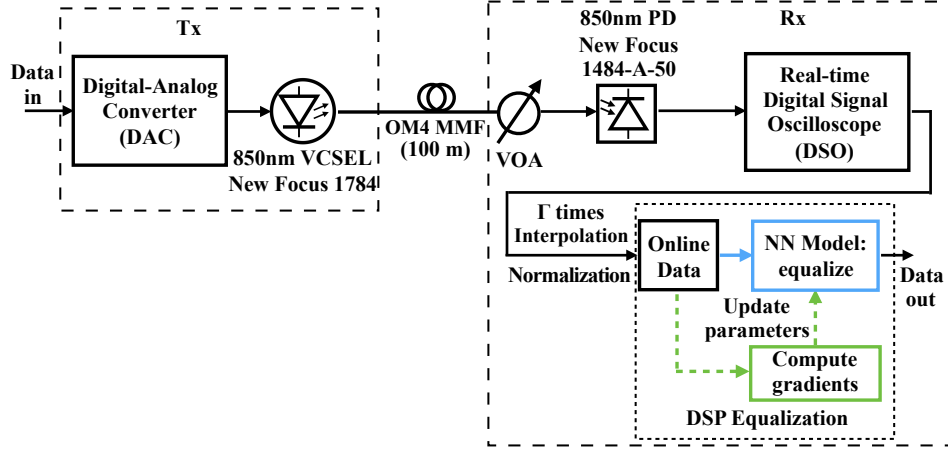


Fig. 5: Experimental configuration of the 56 Gbps PAM-4 signal transmission system utilizing 850-nm VCSEL and OM4 MMF. The input data is generated with Bit-pattern Generator (BPG) using random pattern (56 Gb/s). Since no training sequences are provided, AdaNN updates the parameters online in an unsupervised manner.

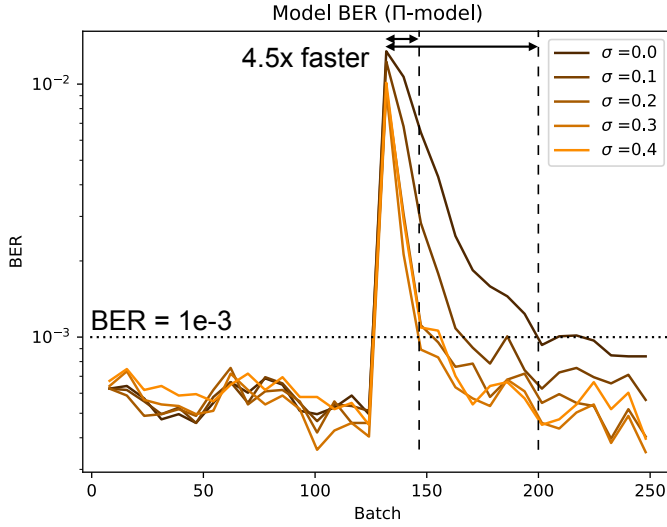


Fig. 6: The BER performance of AdaNN with Π model as loss function, following chronological order. Different curves corresponds to different σ , which is the standard deviation of added Gaussian noise in $g_{\sigma}(\cdot)$.

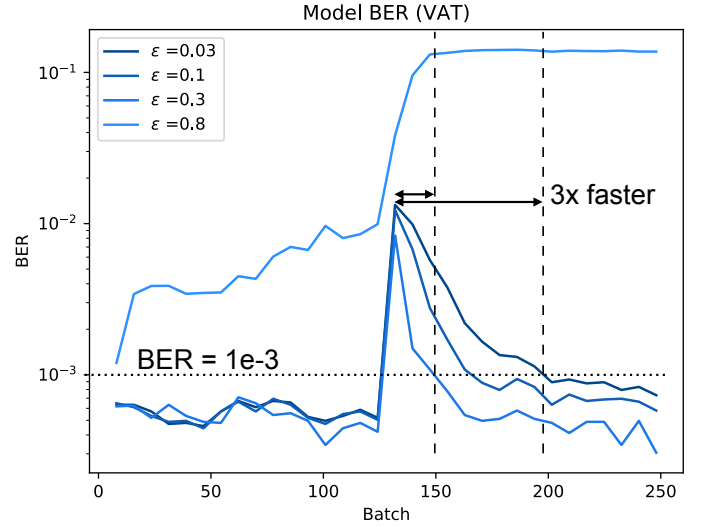


Fig. 7: The BER performance of AdaNN with VAT as loss function, following chronological order. Different curves corresponds to different ϵ , which is the L_2 -norm of adversarial perturbation \mathbf{r}_{adv} .

one is the convergence time, defined as the number of batches it takes before reaching a BER lower than 10^{-3} ; the other is final BER value at the end of online training stage. The batch size for online training is fixed to be $N_b = 16384$ ($N_{\text{batch}} = 256$). The influence of N_b will be discussed in Section III.

Fig. 6 gives the BER performance of AdaNN with Π model as the loss function, following chronological order. The BER curves have been smoothed in order to facilitate comparison. σ describes the magnitude of Gaussian noise added. Note that vanilla self-training is identical to Π model with $\sigma = 0$. Taking advantage of data augmentation, AdaNN with Π -model as loss function can be 4.5 times faster than self-training, which is a simple imitation of decision-directed adaptive equalization.

Fig. 7 gives the BER performance of AdaNN with VAT as loss function. The hyper-parameter ξ in Algorithm 1, which is the step size of gradient estimation, is fixed as $\xi = 0.1$. On the other hand, ϵ , which denotes the length of

adversarial perturbation \mathbf{r}_{adv} , is changed. The results show that when considering convergence time, AdaNN with VAT as loss function can be 3 times faster than self-training.

Fig. 8 gives the BER performance of AdaNN with Aug-VAT as loss function. Combined with data-augmentation, AdaNN with Aug-VAT converges slightly faster than AdaNN with VAT. The final BER is also lower, indicating that stochastic data augmentation can improve VAT's performance further.

We now summarize the convergence time as well as final BER when using the above 4 different loss functions. The results are given in Table. I. The numbers in bold represents the best performance among one class of training method (only hyper-parameters are changed). Red values means achieving the best BER performance among all listed training schemes, while blue values means being in the second place. Table. I illustrates that AdaNN with Aug-VAT is stably superior than AdaNN with other loss functions. While

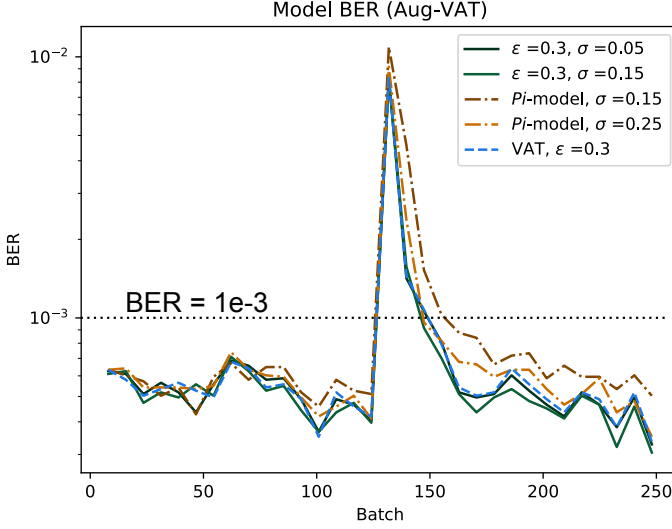


Fig. 8: The BER performance of AdaNN with Aug-VAT as loss function, following chronological order. Different curves corresponds to different σ , which is the L_2 -norm of adversarial perturbation \mathbf{r}_{adv} . Note that the BER curves (the dashed lines) of AdaNN with Π -model and VAT are also given.

TABLE I: Convergence time as well as BER performance of AdaNN, with several different loss functions, including self-training, Π -model, VAT, and Aug-VAT. “N/A” means the final BER is still above 10^{-3} .

Training method	Convergence time (batch)	Final BER
Self-training	72	8.39×10^{-4}
Π -model ($\sigma = 0.10$)	40	5.65×10^{-4}
Π -model ($\sigma = 0.15$)	32	4.96×10^{-4}
Π -model ($\sigma = 0.20$)	24	4.04×10^{-4}
Π -model ($\sigma = 0.25$)	24	3.66×10^{-4}
Π -model ($\sigma = 0.30$)	16	3.51×10^{-4}
Π -model ($\sigma = 0.40$)	32	3.97×10^{-4}
VAT ($\epsilon = 0.03$)	72	7.32×10^{-4}
VAT ($\epsilon = 0.10$)	40	5.80×10^{-4}
VAT ($\epsilon = 0.20$)	24	4.43×10^{-4}
VAT ($\epsilon = 0.30$)	24	3.36×10^{-4}
VAT ($\epsilon = 0.80$)	N/A	1.37×10^{-1}
Aug-VAT ($\sigma = 0.05, \epsilon = 0.30$)	24	3.20×10^{-4}
Aug-VAT ($\sigma = 0.10, \epsilon = 0.30$)	16	3.13×10^{-4}
Aug-VAT ($\sigma = 0.15, \epsilon = 0.30$)	16	3.05×10^{-4}
Aug-VAT ($\sigma = 0.20, \epsilon = 0.30$)	16	3.51×10^{-4}
Aug-VAT ($\sigma = 0.30, \epsilon = 0.30$)	16	3.89×10^{-4}

self-training suffers from slow convergence, AdaNN with Aug-VAT can be 4.5 times faster, which indicates AdaNN’s effective usage of unlabeled data.

There’re several other different loss functions we haven’t cover. “Temporal ensemble” [24] requires re-evaluation of all training samples each time the NN parameters are updated. That’s too costly for online training. “Mean teacher” [33] constructs an ensemble using current model and several past models during training. Experiments show that although being complicated, “Mean teacher” has no significant difference compared with self-training when tested on our task. We also know that many semi-supervised learning algorithms are based on “low dimension manifold assumption”, which assumes that data lie approximately on a manifold of much lower dimension compared with input space. Relevant algorithms include low

dimension manifold model (LDMM) and curvature regularization (CURE) [34], [35]. By adding regularization terms these algorithms have achieved good performance. However the estimation of local dimension/curvature requires access to all data points in a small area, which cannot be guaranteed at online stage.

D. Different optimizers

In the previous part, we’ve used Momentum SGD without discussing other optimization algorithms. Researchers have proposed many first-order optimization algorithms (also known as “optimizers”). Several influential optimizers include: SGD [36], Momentum SGD [37], Nesterov Momentum [38], AdaGrad [39], RMSprop [26], and Adam [40]. Although generally Adam leads to faster convergence at the early stage of training, it has been reported that Momentum SGD can often yield better results compared with Adam under the condition that they’re both fully trained [41]. Due to its stability, we’ve used Momentum SGD in the previous part. However, the advantages and disadvantages of different optimizers rely on the task, and researchers have not reached final conclusion on “which optimizer is the best”. In this part we’re focusing on: SGD, Momentum SGD, AdaGrad and Adam, since they are also used in [42]. The differences between these four optimizers are given in this part. Recall from Eq. (8) that all these optimizers can be written uniformly as

$$\theta_{t+1} = \theta_t - \frac{\alpha_t}{\psi(\mathbf{g}_1, \dots, \mathbf{g}_t)} \phi(\mathbf{g}_1, \dots, \mathbf{g}_t), \quad (12)$$

where \mathbf{g}_k represents the gradient obtained in the k -th time step, $\alpha_t/\psi(\mathbf{g}_1, \dots, \mathbf{g}_t)$ denotes the adaptive learning rate, and $\phi(\mathbf{g}_1, \dots, \mathbf{g}_t)$ is the gradient estimation.

1) *Vanilla SGD:* By choosing $\alpha_t = \alpha$, $\psi(\mathbf{g}_1, \dots, \mathbf{g}_t) = 1$ and $\phi(\mathbf{g}_1, \dots, \mathbf{g}_t) = \mathbf{g}_t$, Eq. (8) leads to the vanilla SGD:

$$\theta_{t+1} = \theta_t - \alpha \cdot \mathbf{g}_t. \quad (13)$$

2) *SGD with Momentum:* By choosing $\alpha_t = \alpha$, $\psi(\mathbf{g}_1, \dots, \mathbf{g}_t) = 1$ and $\phi(\mathbf{g}_1, \dots, \mathbf{g}_t) = \sum_{i=1}^t \beta^{t-i} \mathbf{g}_i$, Eq. (8) leads to Momentum SGD given in Eq. (4):

$$\begin{cases} \mathbf{V}_{t+1} = \beta \mathbf{V}_t - \alpha \cdot \mathbf{g}_t, \\ \theta_{t+1} = \theta_t + \mathbf{V}_{t+1}. \end{cases} \quad (14)$$

3) *AdaGrad:* By choosing $\alpha_t = \alpha$, $\psi(\mathbf{g}_1, \dots, \mathbf{g}_t) = \sqrt{\sum_{i=1}^t \mathbf{g}_i^2} + \epsilon_0$ and $\phi(\mathbf{g}_1, \dots, \mathbf{g}_t) = \mathbf{g}_t$, Eq. (8) leads to the AdaGrad:

$$\begin{cases} \mathbf{G}_t = \mathbf{G}_{t-1} + \mathbf{g}_t^2, \\ \theta_{t+1} = \theta_t - \frac{\alpha}{\sqrt{\mathbf{G}_t + \epsilon_0}} \odot \mathbf{g}_t, \end{cases} \quad (15)$$

where ϵ_0 is small, typically smaller than 10^{-7} . Symbol \odot denotes element-wise product.

4) *Adam:* Adam optimizer is a bit more complicated than AdaGrad:

$$\begin{cases} \mathbf{m}_t = \beta_1 \mathbf{m}_{t-1} + (1 - \beta_1) \mathbf{g}_t, \\ \mathbf{G}_t = \beta_2 \mathbf{G}_{t-1} + (1 - \beta_2) \mathbf{g}_t^2, \\ \hat{\mathbf{m}}_t = \mathbf{m}_t / (1 - \beta_1^t), \\ \hat{\mathbf{G}}_t = \mathbf{G}_t / (1 - \beta_2^t), \\ \theta_{t+1} = \theta_t - \frac{\alpha}{\sqrt{\hat{\mathbf{G}}_t + \epsilon_0}} \odot \hat{\mathbf{m}}_t, \end{cases} \quad (16)$$

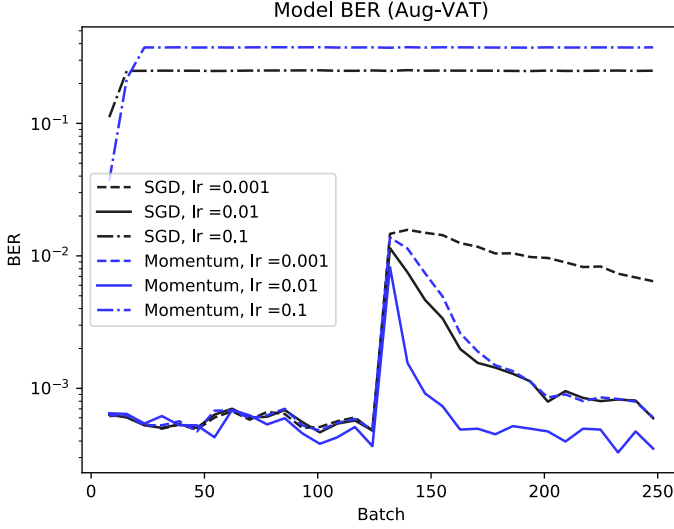


Fig. 9: The BER performance when using two different optimizers, namely SGD and Momentum SGD. It can be concluded that Momentum SGD converges faster compared with SGD. On the other hand, a very large learning rate leads to poor performance.

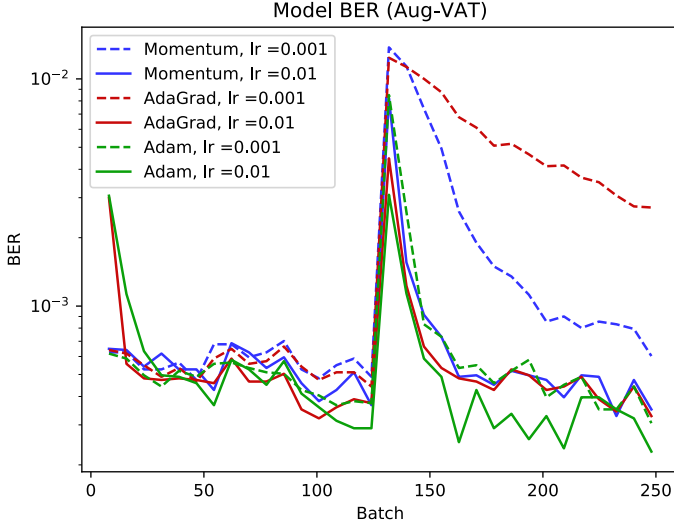


Fig. 10: The BER performance when using two different optimizers with adaptive learning rate, namely AdaGrad and Adam. The BER curve of Momentum SGD is also plotted. The performance of Adam is more stable compared with Momentum SGD and AdaGrad.

where ϵ_0 is typically smaller than 10^{-7} , β_1 and β_2 are constants.

During online training stage, using different optimizers can actually lead to very different BER performance. Fig. 9 gives the BER performance when using vanilla SGD and SGD with momentum. The learning rate is chosen from $\alpha \in \{0.1, 0.01, 0.001\}$. It is obvious that learning rate should be neither too large (fail to converge) nor too small (will be able to converge, but with very slow rate). On the other hand, SGD momentum always converges faster compared with vanilla SGD, which justifies our previous choice. Fig. 10 is also given in order to compare Momentum SGD with two adaptive optimizers, namely AdaGrad and Adam. We find that the performance of Momentum SGD (with $\alpha = 0.01$) is very

similar to that of AdaGrad (with $\alpha = 0.01$), while Adam (with $\alpha = 0.001$, $\beta_1 = 0.9$ and $\beta_2 = 0.999$) is slightly better.

We now summarize the convergence time as well as final BER of the above 4 different optimizers. The results are given in Table. II. The numbers in bold represents the best performance among one optimizer (only learning-rate is changed). Red values means achieving the best BER performance among all listed optimizers, while blue values means being in the second place. We can conclude that: (1) $\alpha = 0.01$ is a suitable learning-rate for most optimizers. (2) While being 4.5 times faster than vanilla SGD, Adam yields slightly better BER performance on the whole. Despite of this, for an optical link whose properties change frequently, the optimizer as well as its learning rate should be chosen more carefully based on experimental results.

III. INFLUENCE OF SLIDING WINDOW STEP SIZE

For our experiments in Section. II, the sliding window step size N_b is fixed as 16384 for $N_{\text{batch}} = 256$, which means both set1 and set2 are divided into 128 mini-batches during online equalization process. Choosing different N_b has an important impact on the online training process. Concretely, N_b describes how many data needs to be collected before AdaNN updates its parameters. A very large N_b makes it impossible to track the changes occur in optical channel. A very small N_b seems plausible since the model parameters are updated frequently. Unfortunately, a very small N_b may cause new problem. To show this, we recall that unlabeled data can facilitate model training since they give information on the probability distribution $p(x)$. A small N_b leads to very small batch containing few data, which does not reflect the overall probability distribution. Take binary classification as an example. Consider an extreme circumstance given in Fig. 11 where all data points in a single batch locate at one side of the decision boundary. Since the NN does not know any label information, all 4 points are classified as “blue” class, and by applying gradient descent, the decision boundary will be pushed towards the opposite direction. As Fig. 11 shows, using very small batches is likely to slow down the convergence speed, and training process may even fail to converge.

Now we are giving BER performance results regarding different N_b . The loss function used here is Aug-VAT, with hyper-parameters $\sigma = 0.15$ and $\epsilon = 0.30$, following the

TABLE II: BER performance for several different optimizers.

Training optimizer	Convergence time (batch)	Final BER
SGD ($\alpha = 10^{-3}$)	N/A	6.44×10^{-3}
SGD ($\alpha = 10^{-2}$)	72	5.95×10^{-4}
SGD ($\alpha = 10^{-1}$)	N/A	2.50×10^{-1}
Momentum ($\alpha = 10^{-3}$)	72	6.03×10^{-4}
Momentum ($\alpha = 10^{-2}$)	16	3.05×10^{-4}
Momentum ($\alpha = 10^{-1}$)	N/A	3.75×10^{-1}
AdaGrad ($\alpha = 10^{-3}$)	N/A	2.72×10^{-3}
AdaGrad ($\alpha = 10^{-2}$)	16	3.28×10^{-4}
AdaGrad ($\alpha = 10^{-1}$)	N/A	3.75×10^{-1}
Adam ($\alpha = 10^{-3}$)	16	3.05×10^{-4}
Adam ($\alpha = 10^{-2}$)	16	2.29×10^{-4}
Adam ($\alpha = 10^{-1}$)	N/A	3.75×10^{-1}

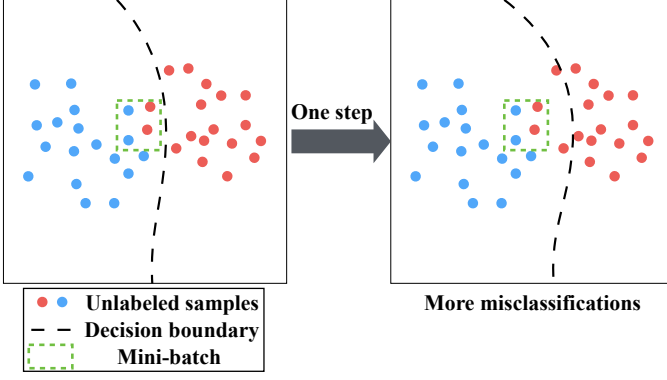


Fig. 11: Demonstration of why choosing very small N_b leads to slow convergence. A batch containing few data points does not reflect the overall probability distribution. The decision boundary, therefore, will be pushed towards wrong direction very often, slowing down the convergence speed.

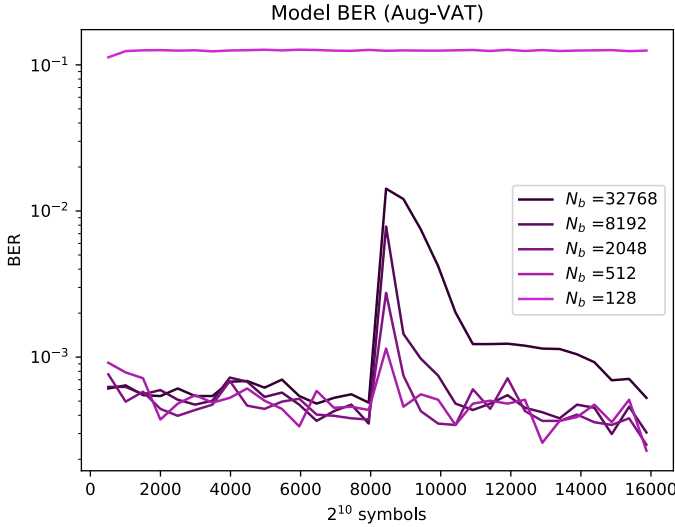


Fig. 12: The BER performance when choosing different N_b , following chronological order. Different curves corresponds to different N_b , which is the batch size. It can be concluded that in order to obtain a faster convergence speed, N_b should be chosen according to the changing speed of link properties.

previous part. Fig. 12 gives the BER performance when N_b takes different values, ranging from 128 to 32768. Generally, a smaller N_b means that the model is updated more frequently, so less data will be needed before the BER performance reaches stability. However, as can be seen from the case $N_b = 128$, when training on very small batch the training process may fail to converge. When building an actual system, the choice of N_b should be neither too large nor too small: it should be specified and tuned manually, depending on how frequently the link properties change.

IV. COMPUTATIONAL COMPLEXITY

In this section, we focus on analyzing the computational cost of proposed AdaNN. Fully-connected NNs mainly involve two types of computations: multiplications and activation functions. Note that here rather than $\tanh(\cdot)$, ReLU activation function is used. Therefore when analyzing computational complexity, we don't need to consider activation function,

which is different from [19]. For a non-adaptive deep neural network, the calculation of output probability vector \mathbf{o} is called “forward propagation”, which follows Eq. (1)(2). When equalizing a single symbol, each layer can be viewed as a vector. Denote the interpolation multiple as Γ , and the number of neurons contained in all l_{NN} layers are: $\Gamma(2L+1)$, R , R , ..., R , and M . The number of floating-point multiplications k_{NN} can be calculated as

$$k_{\text{NN}} = \Gamma(2L+1) \cdot R + (l_{\text{NN}} - 3) \cdot R^2 + R \cdot M. \quad (17)$$

As for AdaNN, in addition to forward propagation, all the parameters (including both weights and biases) need to be adjusted online, based on gradients $\nabla_{\mathbf{W}_k} L_{\text{loss}}$ and $\nabla_{\mathbf{b}_k} L_{\text{loss}}$. According to [26], all these gradients are calculated by implementing back-propagation algorithm, which is given in Algorithm 3.

Algorithm 3 Backward propagation

Require: l_{NN} = the number of layers in the network
Require: $\mathbf{W}_k, k \in \{1, \dots, l_{\text{NN}} - 1\}$ = weight matrices of all layers
Require: $\mathbf{b}_k, k \in \{1, \dots, l_{\text{NN}} - 1\}$ = bias vectors of all layers
Require: \mathbf{v} = the input feature vector
1: $\mathbf{g} \leftarrow \nabla_{\mathbf{o}} L_{\text{loss}} \triangleright$ last layer
2: **for** $k = l_{\text{NN}} - 1, \dots, 1$ **do**
3: $\mathbf{g} \leftarrow \nabla_{\mathbf{a}_k} L_{\text{loss}} = \mathbf{g} \odot \sigma'(\mathbf{a}_k) \triangleright \sigma'(x) = 1$ if and only if $x > 0$
4: $\nabla_{\mathbf{b}_k} L_{\text{loss}} = \mathbf{g}$
5: $\nabla_{\mathbf{W}_k} L_{\text{loss}} = \mathbf{g} \mathbf{h}_{k-1}^\top$
6: $\mathbf{g} \leftarrow \nabla_{\mathbf{h}_{k-1}} L_{\text{loss}} = \mathbf{W}_k^\top \mathbf{g} \triangleright$ continue to layer $k - 1$
7: **end for**

Consider the back-propagation from layer k to layer $k - 1$. The number of neurons contained in each layer can be denoted as R_k and R_{k-1} . It's straightforward to see that, during the back-propagation from layer k to layer $k - 1$, $\mathbf{g} \leftarrow \mathbf{g} \odot \sigma'(\mathbf{a}_k)$ requires R_k multiplications, $\nabla_{\mathbf{W}_k} L_{\text{loss}} = \mathbf{g} \mathbf{h}_{k-1}^\top$ requires $R_{k-1} \cdot R_k$ multiplications, and $\mathbf{g} \leftarrow \mathbf{W}_k^\top \mathbf{g}$ requires $R_{k-1} \cdot R_k$ multiplications. By summing over all layers, we can conclude that for a single back-propagation, the number of required floating-point multiplications k_{back} can be calculated as

$$\begin{aligned} k_{\text{back}} &= [2\Gamma(2L+1) \cdot R + R] \\ &\quad + (l_{\text{NN}} - 3) \cdot (2R^2 + R) + (2R \cdot M + M) \quad (18) \\ &= 2k_{\text{NN}} + (l_{\text{NN}} - 2) \cdot R + M. \end{aligned}$$

The computational cost of back-propagation is slightly larger than two times the computational cost of forward propagation.

When Π -model serves as loss function, two forward propagations and one back-propagation are needed in a single iteration. Therefore the computational cost of AdaNN (with Π -model as loss function) should be slightly larger than four times the computational cost of a non-adaptive NN-based equalizer. On the other hand, when Aug-VAT serves as loss function, two forward propagations, one back-propagation and computing \mathbf{r}_{vadv} (mainly includes one extra forward propagation and one back-propagation) are needed in a single iteration. In total, the computational cost of AdaNN (with

Aug-VAT as loss function) should be slightly larger than seven times the cost of non-adaptive NN. As a contrast, the computational cost of AdaNN (with self-training as loss function) is three times the cost of non-adaptive NN. From Table. I we already know that compared with self-training, AdaNN (with Aug-VAT) needs 4.5 times less iterations before reaching convergence. Therefore the total CPU time Aug-VAT needs before convergence is approximately 52% (calculated using $(7/3) \div 4.5 \approx 0.5185$) of the time self-training needs.

Note that if we take into account that the back-propagation processes of different samples in the same batch are completely independent of each other, multiple samples can be processed in a paralleled manner, so that the computational time can be greatly reduced with the help of specially designed hardware.

V. EXPERIMENTAL RESULTS

In this section, the evaluation and analysis for the BER performance of AdaNN (using Aug-VAT) and several other equalizers (non-adaptive or adaptive) is conducted. The experimental conditions have already been stated in section II. The only difference is that during online training stage, Adam optimizer (initial learning rate $\alpha = 0.01$, $\beta_1 = 0.9$, $\beta_2 = 0.999$) is used.

A. Compare: Non-Adaptive NN

The BER performance of AdaNN as well as a normal NN-based equalizer is given in Fig. 13. Note that to ensure fairness, the network structure of NN is exactly the same as that of AdaNN (given in Fig. 1). Before online equalization, both AdaNN and the NN are trained offline using 25% data in set1 (received optical power -2.7 dBm), so it's reasonable that both equalizers perform well when processing set1. When processing set2, the BER of NN rises to about 1.6×10^{-2} abruptly, and remains almost unchanged since it's a non-adaptive model. For AdaNN, the BER also rises when first encountering signals from set2. As the AdaNN model converges, the BER soon drops and ends up similar to the previous level (below 10^{-3}). Note that this training process only takes about 40 batches before the BER stabilizes again.

We've also tested another AdaNN model, which is initially trained offline using a dataset different from set1. The main difference is that the receive optical power (ROP) of the new dataset is -4.7 dBm, so its signal-to-noise ratio (SNR) is lower than set1. This means that AdaNN (trained@ -4.7 dBm) has never received any label for set1 or set2. Surprisingly, compared with AdaNN (trained@ -2.7 dBm), AdaNN (trained@ -4.7 dBm) can achieve very similar BER performance. This indicates that the adaptive training process of AdaNN is robust even when a different offline-trained model is used.

B. Compare: NN with few Labels Provided

In the previous parts, we've already demonstrated that AdaNN is able to adjust its parameters without the help of labels. It's still necessary to investigate the BER performance

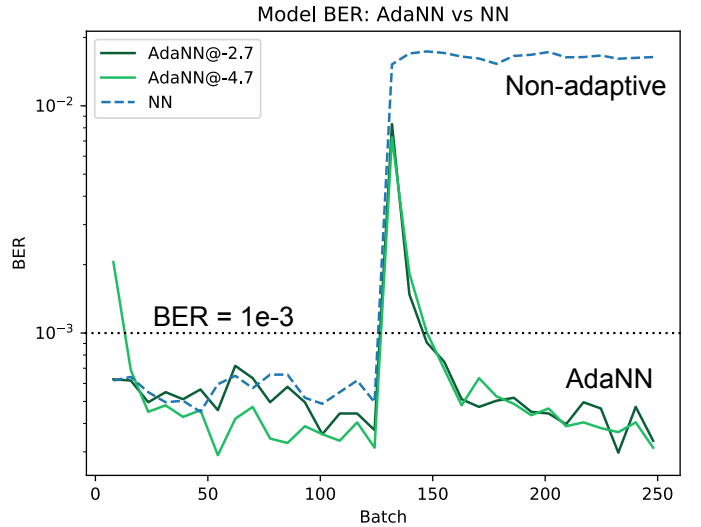


Fig. 13: The BER performance of normal NN-based equalizer, compared with AdaNN. Without online parameter fine-tuning, normal NN suffers from severe performance degradation when the link properties change. Note that performance of AdaNN trained with a different dataset (received optical power is -4.7 dBm) is also plotted, in order to show AdaNN's robustness towards different SNR.

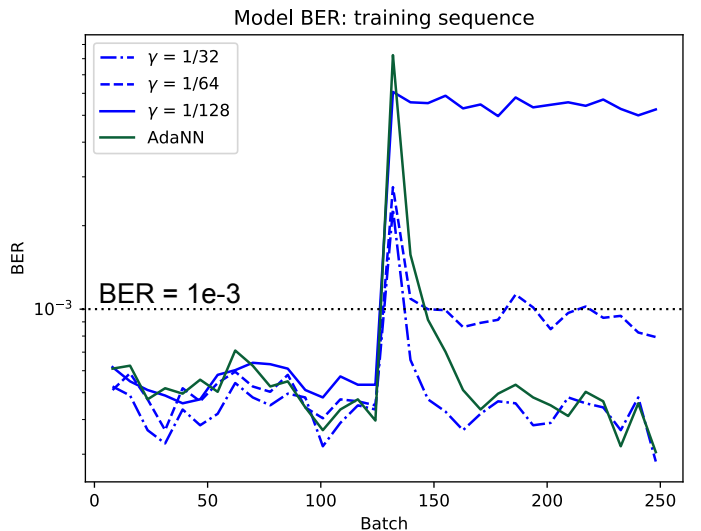


Fig. 14: The BER performance of normal NN-based equalizer, trained in a supervised manner. The parameter γ denotes the proportion of training sequence.

of NN-based equalizers when short training sequence can be provided.

In this part, assume that two training sequences are provided at the beginning of set1 and set2 respectively. The NN-based equalizer is trained on the training sequences for 100 iterations, ensuring good convergence. Denote the ratio of training sequence length to set1 length (or set2 length) as γ . Fig. 14 shows the BER results of NN-based equalizer, fine-tuned with provided training sequence. If γ is larger than $1/32$, the BER performance is slightly better than AdaNN. For smaller values of γ , however, the performance degradation becomes unacceptable.

Note that researchers in the field of wireless communication are also exploring possible applications of deep learn-

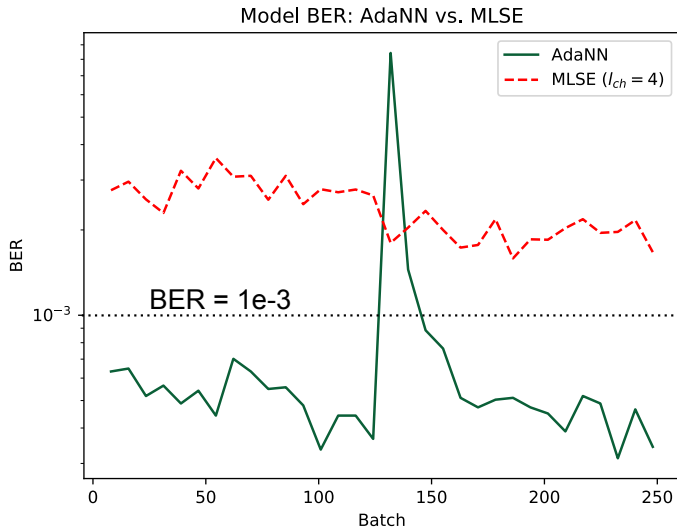


Fig. 15: The BER performance of AdaNN and conventional MLSE. For MLSE, the channel response coefficients are updated online using LMS algorithm.

ing techniques [43]-[47]. However they still rely on pilots when the model parameters are changed adaptively [43]. In [48], the authors claimed that channel estimation based on semi-supervised learning or unsupervised learning is still an open subject. Our experimental results show that AdaNN can achieve better (at least similar) BER performance compared with NN-based equalizer, even when a portion of labels are provided to that NN. There are cases when sending extra training sequence is not supported, or when the cost of providing training sequence becomes unacceptable. Based on semi-supervised learning, AdaNN needs no training sequence and thus provides an effective alternative for these occasions.

C. Compare: Conventional MLSE

We have also compared AdaNN with conventional MLSE. The length of channel response is fixed as $l_{ch} = 4$. The channel response coefficients are estimated using least mean square (LMS) algorithm. Note that the true labels are provided when updating these coefficients, indicating that here MLSE works adaptively in a supervised manner. The update frequency of channel response coefficients is exactly the same as the update frequency of AdaNN parameters. The BER performance of both AdaNN and MLSE are given in Fig. 15. Although AdaNN takes more iterations to converge after the link properties change (because the NN model contains more parameters), the final BER of AdaNN (3.0×10^{-4}) is still much lower than that of MLSE (2.4×10^{-3}). The results show that by using this efficient online training scheme, the generalization ability of NN-based equalizer can be stronger compared with adaptive conventional algorithms.

VI. CONCLUSION

In this paper, we propose an adaptive online training scheme, which can be used to fine-tune NN-based equalizer without the help of training sequence. The proposed adaptive NN-based equalizer is called “AdaNN”. At the online stage,

recently received data are collected using a sliding-window. With the help of unlabeled data, all the parameters in our NN are fine-tuned in an unsupervised manner, which is similar to decision-directed adaptive equalization. The performance of AdaNN is evaluated in a 56 Gb/s PAM4-modulated VCSEL optical link, where the VCSEL is turned off and on after transmitting half the data. Our experimental results indicate that by introducing AdaNN, the BER performance can be improved compared with both non-adaptive NN-based equalizers and conventional MLSE. The convergence speed of AdaNN with Aug-VAT is 4.5 times faster compared with a simple decision-directed adaptive NN. The online training process has been proved robust when different offline-trained models are used, which shows AdaNN’s wide availability. The computational complexity of AdaNN training scheme is also analyzed theoretically, showing that compared with vanilla self-training, the CPU time it requires before convergence can be reduced by 50% when using Aug-VAT loss function. We can conclude that it is feasible to construct adaptive NN-based equalizer with acceptable computational cost when training sequences aren’t provided. The generalization ability of all NN-based equalizers can be greatly improved using our proposed method.

REFERENCES

- [1] D. Kuchta, A. Rylyakov, F. Doany, C. Schow, J. Proesel, C. Baks, and A. Larsson, “A 71 Gb/s NRZ modulated 850-nm VCSEL-based optical link,” *IEEE Photon. Technol. Lett.*, vol. 27, no. 6, pp. 577-580, Jan. 2015.
- [2] D. Kuchta, “Higher speed VCSEL links using equalization”, *presented at the European Conf. on Optical Communication*, Düsseldorf, Germany, 2016, Paper Tu.1.A.2.
- [3] Z. Tan, C. Yang, Y. Zhu, Z. Xu, K. Zou, F. Zhang, and Z. Wang, “High speed band-limited 850-nm VCSEL link based on time-domain interference elimination,” *IEEE Photon. Technol. Lett.*, vol. 29, no. 9, pp. 751-754, May. 2017.
- [4] F. Karinou *et al.*, “Experimental performance evaluation of equalization techniques for 56 Gb/s PAM-4 VCSEL-based optical interconnects,” *presented at the European Conf. on Optical Communication*, Valencia, Spain, 2015, Paper P.4.10.
- [5] T. Lengyel, K. Szczerba, P. Westbergh, M. Karlsson, A. Larsson, and P. Andrekson, “Sensitivity improvements in an 850-nm VCSEL-based link using a two-tap pre-emphasis electronic filter,” *J. Lightw. Technol.*, vol. 35, no. 9, pp. 1633-1639, Dec. 2016.
- [6] K. Szczerba, T. Lengyel, M. Karlsson, P. Andrekson, and A. Larsson, “94 Gb/s 4-PAM using an 850-nm VCSEL, pre-emphasis, and receiver equalization,” *IEEE Photon. Technol. Lett.*, vol. 28, no. 22, pp. 2519-2521, Nov. 2016.
- [7] J. Lavrencik, V. Thomas, S. Varughese, and S. Ralph, “DSP-enabled 100 Gb/s PAM-4 VCSEL MMF links,” *J. Lightw. Technol.*, vol. 35, no. 15, pp. 31893196, Aug. 2017.
- [8] Y. Gao, F. Zhang, L. Dou, Z. Chen, and A. Xu, “Intra-channel nonlinearities mitigation in pseudo-linear coherent QPSK transmission systems via nonlinear electrical equalizer,” *Opt. Commun.*, vol. 282, no. 12, pp. 2421-2425, Jun. 2009.
- [9] L. Ge, W. Zhang, C. Liang, and Z. He, “Threshold based pruned retraining Volterra equalization for 100 Gbps/lane and 100m optical interconnects based on VCSEL and MMF,” *J. Lightw. Technol.*, vol. 37, no. 13, pp. 3222-3228, Apr. 2019.
- [10] S. Lu *et al.*, “81.7% complexity reduction of Volterra nonlinear equalizer by adopting L1 regularization penalty in an OFDM long-reach PON,” *presented at the European Conf. on Optical Communication*, Gothenburg, Sweden, 2017, Paper P1.SC3.38.
- [11] E. Ip, and J. Kahn, “Compensation of dispersion and nonlinear impairments using digital backpropagation,” *J. Lightw. Technol.*, vol. 26, no. 20, pp. 3416-3425, Oct. 2008.
- [12] R. Dar, M. Feder, A. Mecozzi, and M. Shtaf, “Inter-channel nonlinear interference noise in WDM systems: Modeling and mitigation,” *J. Lightw. Technol.*, vol. 33, no. 5, pp. 1044-1053, Dec. 2014.

- [13] C. Li, F. Zhang, Y. Zhu, M. Jiang, Z. Chen, and C. Yang, "Fiber nonlinearity mitigation in single carrier 400 G and 800 G Nyquist-WDM systems," *J. Lightw. Technol.*, vol. 36, no. 17, pp. 3707-3715, Sep. 2018.
- [14] T. O'Shea, J. Hoydis, "An introduction to deep learning for the physical layer," *IEEE Trans. Cogn. Commun. Netw.*, vol. 3, no. 4, pp. 563-575, Dec. 2017.
- [15] J. Estaran *et al.*, "Artificial neural networks for linear and non-linear impairment mitigation in high-baudrate IM/DD systems," *presented at the European Conf. on Optical Communication*, Düsseldorf, Germany, 2016, Paper M.2.B.2.
- [16] C. Chuang *et al.*, "Employing deep neural network for high speed 4-PAM optical interconnect," *presented at the European Conf. on Optical Communication*, Gothenburg, Sweden, 2017, Paper W.2.D.2.
- [17] C. Chuang *et al.*, "Convolutional neural network based nonlinear classifier for 112-Gbps high speed optical link," *presented at the Optical Fiber Communication Conf.*, San Diego, CA, USA, 2018, Paper W2A.43.
- [18] C. Ye *et al.*, "Recurrent neural network (RNN) based end-to-end non-linear management for symmetrical 50Gbps NRZ PON with 29dB+ loss budget," *presented at the European Conf. on Optical Communication*, Rome, Italy, 2018, Paper Mo4B.3.
- [19] Q. Zhou, C. Yang, A. Liang, X. Zheng, and Z. Chen, "Low computationally complex recurrent neural network for high speed optical fiber transmission," *Opt. Commun.*, vol. 441, pp. 121-126, Jun. 2019.
- [20] B. Karanov, M. Chagnon, F. Thouin, T. Eriksson, H. Bülow, D. Lavery, P. Bayvel, and L. Schmalen, "End-to-end deep learning of optical fiber communications," *J. Lightw. Technol.*, vol. 36, no. 20, pp. 4843-4855, Oct. 2018.
- [21] T. Eriksson, H. Bülow, and A. Leven, "Applying neural networks in optical communication systems: possible pitfalls," *IEEE Photon. Technol. Lett.*, vol. 29, no. 23, pp. 2091-2094, Dec. 2017.
- [22] X. Zhu, "Semi-supervised learning literature survey," University of Wisconsin-Madison, Department of Computer Sciences, 2005. [Online]. Available at: <https://minds.wisconsin.edu/handle/1793/60444>.
- [23] D. Lee, "Pseudo-label: The simple and efficient semi-supervised learning method for deep neural networks," in *Workshop on Challenges in Representation Learning, ICML*, 2013.
- [24] S. Laine, T. Aila, "Temporal ensembling for semi-supervised learning," in *Proc. Int. Conf. on Learning Representations (ICLR)*, 2017.
- [25] T. Miyato, S. Maeda, S. Ishii, and M. Koyama, "Virtual adversarial training: a regularization method for supervised and semi-supervised learning," *IEEE Trans. Pattern Anal.*, Jul. 2018.
- [26] I. Goodfellow, Y. Bengio, and A. Courville, *Deep Learning*, the MIT Press, 2016.
- [27] I. Goodfellow, J. Shlens, and C. Szegedy, "Explaining and harnessing adversarial examples," in *Proc. Int. Conf. on Learning Representations (ICLR)*, 2015.
- [28] H. Huang, C. Wang, and B. Dong, "Nostalgic Adam: Weighting more of the past gradients when designing the adaptive learning rate," *arXiv preprint arXiv:1805.07557*, Feb. 2019.
- [29] A. Liang, C. Yang, C. Zhang, Y. Liu, F. Zhang, Z. Zhang, and H. Li, "Experimental study of support vector machine based nonlinear equalizer for VCSEL based optical interconnect," *Opt. Commun.*, vol. 427, pp. 641647, Nov. 2018.
- [30] Newport, 1784 VCSEL Datasheet, 2017. [Online]. Available at: <https://www.newport.com.cn/p/1784>.
- [31] Newport, 1484-A-50-User's Manual, 2017. [Online]. Available at: <https://www.newport.com/p/1484-A-50>.
- [32] Keras Documentation, 2015. [Online]. Available at: <https://keras.io>.
- [33] A. Tarvainen, and H. Valpola, "Mean teachers are better role models: Weight-averaged consistency targets improve semi-supervised deep learning results," in *Advances in neural information processing systems (NIPS)*, pp. 1195-1204, 2017.
- [34] S. Osher, Z. Shi, and W. Zhu, "Low dimensional manifold model for image processing," *SIAM J. Imaging. Sci.*, vol. 10, no. 4, pp. 1669-1690, Oct. 2017.
- [35] B. Dong, H. Ju, Y. Lu, and Z. Shi, (2019). "CURE: Curvature Regularization for missing data recovery," *arXiv preprint arXiv:1901.09548*, May. 2019.
- [36] H. Robbins, and S. Monro, "A stochastic approximation method," *Ann. Math. Stat.*, pp. 400-407, Sep. 1951.
- [37] D. Rumelhart, G. Hinton, and R. Williams, "Learning representations by back-propagating errors," *Nature*, vol. 323, pp. 533-536, Oct. 1986.
- [38] I. Sutskever, J. Martens, G. Dahl, G. Hinton, "On the importance of initialization and momentum in deep learning," in *Proc. Int. Conf. on Machine Learning (ICML)*, pp. 1139-1147, 2013.
- [39] J. Duchi, E. Hazan, and Y. Singer, "Adaptive subgradient methods for online learning and stochastic optimization," *J. Mach. Learn. Res.*, vol. 12, pp. 2121-2159, Jul. 2011.
- [40] D. Kingma, and J. Ba, "Adam: a method for stochastic optimization," in *Proc. Int. Conf. on Learning Representations (ICLR)*, 2015.
- [41] A. Wilson *et al.*, "The marginal value of adaptive gradient methods in machine learning," in *Advances in neural information processing systems (NIPS)*, pp. 4148-4158, 2017.
- [42] A. Zappone, M. Renzo, and M. Debbah, "Wireless networks design in the era of deep learning: model-based, AI-based, or both?" *arXiv preprint arXiv:1902.02647*, Jun. 2019.
- [43] H. Ye, G. Li, and B. Juang, "Power of deep learning for channel estimation and signal detection in OFDM systems," *IEEE Wireless. Commun. Lett.*, vol. 7, no. 1, pp. 114-117, Sep. 2017.
- [44] H. Ye, L. Liang, G. Li, and B. Juang, "Deep learning based end-to-end wireless communication systems with conditional GAN as unknown channel," *arXiv preprint arXiv:1903.02551*, Mar. 2019.
- [45] J. Zhang *et al.*, "Deep learning based on orthogonal approximate message passing for CP-free OFDM," in *IEEE Int. Conf. on Acoustics, Speech and Signal Processing (ICASSP)*, pp. 8414-8418, 2019.
- [46] V. Raj, S. Kalyani, "Backpropagating through the air: Deep learning at physical layer without channel models," *IEEE Commun. Lett.*, vol. 22, no. 11, pp. 2278-2281, Nov. 2018.
- [47] T. O'Shea, T. Roy, N. West, and B. Hilburn, "Physical layer communications system design over-the-air using adversarial networks," in *European Signal Processing Conf. (EUSIPCO)*, pp. 529-532, 2018.
- [48] E. Balevi, and J. Andrews, "Deep learning-based channel estimation for high-dimensional signals," *arXiv preprint arXiv:1904.09346*, Apr. 2019.